METTL14 Promotes Lipid Metabolism Reprogramming and Sustains Nasopharyngeal Carcinoma Progression via Enhancing m6A Modification of ANKRD22 mRNA

Wei Xiong (xiongwei@csu.edu.cn)
Key Laboratory of Carcinogenesis and Cancer Invasion of the Chinese Ministry of Education, Cancer Research Institute, Central South University,China
https://orcid.org/0000-0003-1635-8173

Lvyuan Li
Key Laboratory of Carcinogenesis and Cancer Invasion of the Chinese Ministry of Education, Cancer Research Institute, Central South University,China

Qiling Tang
Key Laboratory of Carcinogenesis and Cancer Invasion of the Chinese Ministry of Education, Cancer Research Institute, Central South University,China

Junshang Ge
Key Laboratory of Carcinogenesis and Cancer Invasion of the Chinese Ministry of Education, Cancer Research Institute, Central South University,China

Dan Wang
Key Laboratory of Carcinogenesis and Cancer Invasion of the Chinese Ministry of Education, Cancer Research Institute, Central South University,China

Yongzhen Mo
Key Laboratory of Carcinogenesis and Cancer Invasion of the Chinese Ministry of Education, Cancer Research Institute, Central South University, Changsha, Hunan, China

Yumin Wang
Central South University

Fang Xiong
Key Laboratory of Carcinogenesis and Cancer Invasion of the Chinese Ministry of Education, Cancer Research Institute, Central South University

Qijia Yan
Xiangya Hospital

Qianjin Liao
Central South University https://orcid.org/0000-0001-9320-3090

Can Guo
Key Laboratory of Carcinogenesis and Cancer Invasion of the Chinese Ministry of Education, Cancer Research Institute, Central South University, Changsha, Hunan, China https://orcid.org/0000-0001-7414-2050

Fuyan Wang
Key Laboratory of Carcinogenesis and Cancer Invasion of the Chinese Ministry of Education, Cancer Research Institute, Central South University, Changsha, Hunan, China

Ming Zhou
Central South University

Bo Xiang
Central South University https://orcid.org/0000-0003-2641-5434

Zhaoyang Zeng
Hunan Cancer Hospital and the Affiliated Cancer Hospital of Xiangya School of Medicine, Central South University https://orcid.org/0000-0002-0648-0565

Lei Shi
Department of Pathology, the second Xiangya Hospital, Central South University, Changsha, Hunan, China

Pan Chen
Hunan Cancer Hospital

Article

Keywords: Nasopharyngeal carcinoma, METTL14, m6A, ANKRD22, Lipid metabolism reprogramming

Posted Date: January 25th, 2024

DOI: https://doi.org/10.21203/rs.3.rs-3834927/v1

Additional Declarations: There is **NO** Competing Interest.

Abstract

N^6-methyladenosine (m^6A) modification, a prevalent post-transcriptional RNA modification, plays a crucial role in regulating RNA processing and expression, particularly in the context of malignant tumor progression. However, the exploration of m^6A modification in nasopharyngeal carcinoma (NPC) remains very limited. In this study, we revealed a significant upregulation of the core m^6A methyltransferase, methyltransferase-like 14 (METTL14), in NPC, correlating with poor patient prognosis. In vitro and in vivo experiments demonstrated that METTL14 actively promoted the proliferation and metastasis of NPC cells. Significantly, we identified ANKRD22 as a pivotal downstream target regulated by METTL14. METTL14 catalyzed m^6A modification on ANKRD22 mRNA, recognized by the reader IGF2BP2, leading to increased mRNA stability and higher translational efficiency. Moreover, ANKRD22, a metabolism-related protein on mitochondria, interacted with SLC25A1 to enhance citrate transport, elevating intracellular acetyl-CoA content. This dual impact of ANKRD22 promoted lipid metabolism reprogramming and cellular lipid synthesis while upregulating the expression of cell cycle-related genes (GINS3 and POLE2) and cytoskeleton-related genes (PLEK2 and FERMT1) through heightened epigenetic histone acetylation levels in the nucleus. This intricate network facilitated NPC growth and metastasis. Intriguingly, our findings highlighted elevated ANKRD22-mediated histone H3 lysine 27 acetylation (H3K27AC) signals near the METTL14 promoter, contributing to a positive feedback loop that perpetuated the malignant progression of NPC. The identified METTL14-ANKRD22-SLC25A1 axis emerges as a promising therapeutic target for NPC, and also these molecules may serve as novel diagnostic biomarkers.

Introduction

Nasopharyngeal carcinoma (NPC) is a malignancy originating in the nasopharyngeal mucosa, predominantly prevalent in East and Southeast Asia [1]. The etiology of NPC involves factors such as Epstein-Barr virus (EBV) infection [2], genetic background [3, 4], environment influences [5], and dietary habits [6]. Due to its inconspicuous onset, subtle early symptoms, and pronounced invasive and proliferative characteristics [7], most patients present with lymph node metastasis when diagnosed [8]. While radiotherapy stands as the primary clinical intervention for NPC [9], the principal challenges lie in recurrence and metastasis, constituting the major causes of treatment failure [10]. The pathogenesis of NPC encompasses numerous abnormalities in gene expression, and the underlying molecular mechanisms remain incompletely elucidated. Recent studies have uncovered the significance of dysregulated N^6-methyladenosine (m^6A) modification on messenger ribonucleic acid (mRNA) in governing gene expression through diverse mechanisms, playing a crucial role in the development of malignant tumors [11–13]. Nevertheless, our current understanding of m^6A modification in the pathogenesis of NPC is quite limited.

m^6A modification involves the methylation of the sixth nitrogen of adenosine and stands out as one of the most prevalent chemical modifications on mRNA in eukaryotic cells [14]. This modification is dynamically regulated primarily by m^6A methyltransferases (writers) and m^6A demethylases (erasers) [15–19]. Subsequently, m^6A-modified mRNA is recognized by various specific m^6A recognition proteins (readers), which determine the fate of mRNA in terms of splicing and processing [20, 21], RNA stability [22–24], and translation efficiency [24, 25]. The key writers of m^6A modification include Wilms tumor 1-associated protein (WTAP), methyltransferase-like 3 (METTL3), and methyltransferase-like 14 (METTL14). In NPC, WTAP-mediated m^6A modification of lncRNA DIAPH1-AS1 has been reported to enhance its stability, thereby promoting NPC growth and metastasis [26]. Additionally, WTAP-mediated m^6A methylation on TEA domain transcription factor 4 (TEAD4) has been linked to enhanced stability, contributing to NPC metastasis and chemotherapy resistance [27]. METTL3 has been identified in mediating m^6A modification of the lncRNA SUCLG2-AS1, subsequently promoting metastasis and radiotherapy resistance in NPC [28]. Through the analysis of NPC Gene Expression Omnibus (GEO) datasets GSE12452 and GSE61218, we observed a significant upregulation of METTL14 in NPC. However, the biological functions and potential regulatory mechanisms of METTL14 in NPC are still unclear.

In this study, we confirmed that the expression of METTL14 was indeed elevated in clinical NPC samples, correlating with poor prognosis in patients. Through both in vivo and in vitro experiments, we demonstrated that METTL14 played a pivotal role in promoting the growth and metastasis of NPC cells. Subsequent analysis of NPC m^6A and gene expression profiling microarray data [29], coupled with functional validation, pinpointed ankyrin repeat domain 22 (ANKRD22) as a key downstream target regulated by METTL14. ANKRD22 was found to interact with the citrate transporter protein solute carrier family 25 member 1 (SLC25A1), fostering the production of acetyl coenzyme A (acetyl-CoA). This, in turn, facilitated lipid metabolic reprogramming and epigenetic modifications. On one hand, ANKRD22 enhanced histone H3 lysine 27 acetylation (H3K27AC) near the promoters of genes involved in cell cycle and cytoskeleton, such as GINS Complex Subunit 3 (GINS3), DNA Polymerase Epsilon 2 (POLE2), Pleckstrin 2 (PLEK2), and FERM Domain Containing Kindlin 1 (FERMT1), thereby promoting proliferation and metastasis of NPC. Simultaneously, ANKRD22 increased H3K27AC near the METTL14 promoter, resulting in the upregulation of METTL14 expression. This intricate regulatory mechanism constituted a positive feedback loop within the METTL14-m^6A-ANKRD22 axis.

Results

METTL14 is highly expressed in NPC and associated with poor prognosis of patients

To explore potential changes in m^6A modification levels in NPC, we initially employed the m^6A dot blot method to assess total RNA m^6A modification levels in three NPC tissue samples and three epithelial tissues from chronic rhinitis patients (utilized as normal controls). Notably, we observed a substantial elevation in RNA m^6A modification levels in NPC compared to non-tumor nasopharyngeal epithelial (NPE) tissues (Fig. 1A). This finding suggests that aberrant m^6A modification might play a role in NPC development, and the increased m^6A levels in NPC could be linked to the crucial involvement of m^6A methyltransferases. Furthermore, analysis of m^6A methyltransferase expression in NPC Gene Expression Omnibus (GEO) datasets GSE12452 and GSE61218 revealed a significant upregulation in the mRNA expression of the core m^6A methyltransferase METTL14 in NPC tissues, with no prior published reports on this observation (Fig. 1B). To validate METTL14 expression in NPC tissues, RT-qPCR was conducted on 28 NPC tissues and 7 chronic inflammation tissues of the nasopharynx, confirming heightened METTL14 mRNA expression in NPC tissues (Fig. 1C). Immunohistochemistry (IHC) performed on paraffin sections of 80 NPC and 42 adjacent non-tumor NPE tissues demonstrated elevated METTL14 protein expression in NPC tissues (Fig. 1D). Importantly, the heightened

expression of METTL14 correlated positively with a poorer prognosis in NPC patients (Fig. 1E). Immunofluorescence (IF) and nuclear-cytoplasmic fractionation assays illustrated predominant localization of METTL14 in the nucleus (Fig. 1F-G). Collectively, these findings suggest that the increased expression of METTL14 may significantly contribute to the elevation in m^6A levels in NPC, potentially fostering the development of NPC through m^6A modification.

METTL14 promotes the proliferation and metastasis of NPC cells in vitro and in vivo

To investigate the involvement of METTL14 in NPC development, we designed and synthesized two siRNA sequences (siMETTL14-1, siMETTL14-2) to downregulate METTL14 expression in NPC cells. Conversely, we utilized a METTL14 overexpression vector (pcDNA3.0-METTL14) to induce METTL14 overexpression (Supplementary Fig. 1A-B). m^6A dot blot assays confirmed that siRNA-mediated knockdown of METTL14 significantly reduced RNA m^6A levels in NPC cells, whereas METTL14 overexpression elevated cellular RNA m^6A levels (Fig. 2A). Wound healing assays showed that METTL14 knockdown markedly impeded the migration of NPC cells, while METTL14 overexpression significantly enhanced cell migration (Fig. 2B and Supplementary Fig. 1C). Transwell assays further validated that METTL14 knockdown attenuated the migration and invasion capabilities of NPC cells, whereas METTL14 overexpression increased their migration and invasion abilities (Fig. 2C and Supplementary Fig. 1D). Furthermore, we observed that METTL14 knockdown led to a reduction in the proliferation and colony formation capacity of NPC cells, whereas METTL14 overexpression exerted opposite effects (Supplementary Fig. 1E and Fig. 2D). Altogether, these results strongly indicate that METTL14 plays a pivotal role in promoting the proliferation, migration, and invasion of NPC cells.

To further assess the influence of METTL14 on the growth and metastasis of NPC in vivo, we established subcutaneous tumor model and tail vein lung metastasis model in BALB/C nude mice using NPC cells with either METTL14 overexpression or knockdown. In the subcutaneous tumor model, METTL14 knockdown resulted in a delayed growth of xenograft tumors (Fig. 2E). Compared to the control group, the METTL14 knockdown group exhibited significantly reduced tumor volume (Fig. 2F) and weight (Fig. 2G), while overexpression of METTL14 promoted the growth of the xenograft tumors (Fig. 2E-G). IHC staining revealed a significantly higher expression level of Ki67 in the METTL14 overexpression group compared to the METTL14 knockdown group (Fig. 2H). In the tail vein lung metastasis model, the METTL14 overexpression group displayed a significant increase in the number of lung metastatic nodules compared to the control group, while knocking down METTL14 significantly reduced the number of lung nodules (Fig. 2I-K). These findings collectively suggest that METTL14 promotes the proliferation and metastasis of NPC both in vitro and in vivo.

METTL14 upregulates the expression of ANKRD22 to promote NPC malignant progression

To elucidate the potential mechanism underlying METTL14-mediated promotion of NPC growth and metastasis, we conducted an analysis of m^6A and gene expression profiling microarray data from clinical NPC tissue samples [29]. This dataset encompassed measurements of both m^6A modification levels and mRNA expression levels in NPC clinical samples. A total of 739 genes identified as differentially expressed in NPC tissues, which also exhibited significant changes in m^6A modification levels of their mRNA ($|\log_2 FC| \geq 1$, $p < 0.05$) (Supplementary Fig. 2A). Specifically, 92 genes demonstrated significant upregulation in both m^6A modification status and mRNA expression in NPC tissues (Hyper-up), while 647 genes displayed significant downregulation in both m^6A modification status and mRNA expression (Hypo-down) (Supplementary Fig. 2B and Supplementary Table 7). Since our goal was to identify downstream targets of METTL14, and considering that METTL14 acts as an m^6A-modified writer that is upregulated in NPC, we selected the top 10 significantly upregulated at both m^6A and mRNA levels (ANKRD22, EGFL6, ZIC2, LUZP2, SCNN1G, TMPRSS11F TNFAIP6, CDC6, CLDN1, WNT2) as candidate genes. Subsequently, we investigated the effect of METTL14 on their expressions. Knocking down METTL14 significantly decreased the mRNA expression of ANKRD22 in NPC cells, while overexpression of METTL14 significantly increased the mRNA expression of ANKRD22 (Fig. 3A). In contrast, the expression changes of other genes were not as pronounced (Supplementary Fig. 2C). Consistent with the alterations observed at the RNA level, knocking down METTL14 reduced the protein expression of ANKRD22, while overexpression of METTL14 elevated the protein level of ANKRD22 (Fig. 3B). Further analysis using RT-qPCR on NPC tissues and chronic inflammation tissues of the nasopharynx revealed high expression of ANKRD22 mRNA in NPC tissues (Fig. 3C). IHC results showed that, compared to adjacent non-tumor NPE, ANKRD22 protein was highly expressed in NPC tissues (Fig. 3D). Additionally, patients with high expression of ANKRD22 in NPC exhibited poor overall survival (Fig. 3E). Moreover, the expression of ANKRD22 in NPC tissues was also significantly positively correlated with METTL14 (Supplementary Fig. 2D-E). These findings collectively suggest that METTL14 upregulates the expression of ANKRD22 in NPC.

To probe into the biological role of ANKRD22 in NPC, we employed siRNAs targeting ANKRD22 to knock down its expression and utilized an overexpression vector (pcDNA3.1-ANKRD22) to elevate ANKRD22 expression. RT-qPCR and western blotting confirmed the efficiency of knockdown and overexpression in NPC cell lines (Supplementary Fig. 2F-G). Overexpression of ANKRD22 promoted the migration (Supplementary Fig. 2H-I), invasion (Supplementary Fig. 2I), proliferation (Supplementary Fig. 2J), and colony formation capability (Supplementary Fig. 2K) of NPC cells, while knockdown of ANKRD22 significantly inhibited the migration, invasion, proliferation, and colony formation capability of NPC cells (Supplementary Fig. 2H-K), aligning with the phenotypes observed with METTL14 overexpression or knockdown. Furthermore, in NPC cells, concurrent overexpression of METTL14 and knockdown of ANKRD22 (Supplementary Fig. 3A) revealed that knockdown of ANKRD22 attenuated the METTL14-induced migration (Fig. 3F and Supplementary Fig. 3B) and invasion (Fig. 3G) abilities of NPC cells. MTT and colony formation assays also indicated that knockdown of ANKRD22 inhibited the proliferation (Fig. 3H) and colony formation capability (Fig. 3I) of METTL14-overexpressing NPC cells. Conversely, simultaneous knockdown of METTL14 and overexpression of ANKRD22 in NPC cells (Supplementary Fig. 3C) showed that overexpression of ANKRD22 rescued the decreased cell migration (Supplementary Fig. 3D-E), invasion (Supplementary Fig. 3E), colony formation (Supplementary Fig. 3F), and proliferation (Supplementary Fig. 3G) abilities induced by METTL14 knockdown. These results suggest that METTL14 accelerates the malignant progression of NPC via upregulating ANKRD22.

METTL14 enhances the stability and translation of ANKRD22 mRNA in an m^{6}A-dependent manner

To delve further into the mechanism by which METTL14 regulates ANKRD22 expression in NPC, we treated cells with the transcriptional inhibitor actinomycin D. It revealed that overexpression of METTL14 resulted in a slower degradation of ANKRD22 mRNA, while knockdown of METTL14 accelerated the degradation of ANKRD22 mRNA (Fig. 4A). Additionally, polysome analysis demonstrated that overexpression of METTL14 increased the abundance of ANKRD22 mRNA in the translating pool, while knockdown of METTL14 led to a decrease in ANKRD22 mRNA in the translating pool, with no effect on the translation of the reference gene β-actin (Fig. 4B and Supplementary Fig. 4A). These findings suggest that METTL14 can also promote the translation of ANKRD22.

To test whether METTL14, a methyltransferase for m^{6}A modification, regulates ANKRD22 mRNA through m^{6}A modification, we searched potential m^{6}A modification sites on ANKRD22 mRNA using two independent m^{6}A databases (SRAMP, RMBase) and combined the m^{6}A modification sites shown by m^{6}A and gene expression profiling microarray data [29]. This analysis indicated that the 5' UTR (at positions 130 and 140 nt) of ANKRD22 could be a potential target of METTL14 (Supplementary Fig. 4B).

To validate this finding, we conducted RNA immunoprecipitation (RIP) assays using an anti-METTL14 antibody in CNE2 and HONE1 cells. The results revealed an enrichment of ANKRD22 mRNA by METTL14 (Fig. 4C). MeRIP RT-qPCR further confirmed that knockdown of METTL14 significantly reduced the m^{6}A levels in the 5' UTR of ANKRD22 mRNA in cells (Fig. 4D). Additionally, RNA pull-down assays demonstrated that mutation of the two m^{6}A motifs in the ANKRD22 5' UTR significantly diminished the specific binding of METTL14 to ANKRD22 transcripts (Fig. 4E). Furthermore, mutation of the adenosine (A) to cytosine (C) in both m^{6}A motifs in the 5' UTR of ANKRD22, coupled with luciferase reporter assays, revealed that knockdown of METTL14 substantially reduced the luciferase activity from the wild-type ANKRD22 5' UTR. Conversely, overexpression of METTL14 significantly increased the luciferase activity from the wild-type ANKRD22 5' UTR. Notably, neither knockdown nor overexpression of METTL14 altered the luciferase activity from the mutant ANKRD22 5' UTR (Fig. 4F). These results collectively indicate that METTL14 interacts with the 5' UTR region of ANKRD22, and through an m^{6}A-dependent pathway, METTL14 enhances the stability and translation of ANKRD22 mRNA in NPC cells.

IGF2BP2 recognizes METTL14-mediated m^{6}A modification on ANKRD22 mRNA

m^{6}A modification on mRNA is recognized and bound by m^{6}A reader proteins, which determine the fate of methylated mRNA. Two major families of readers that recognize m^{6}A-modified mRNA have been reported: YTHDF1/2/3 and IGF2BP1/2/3 [30–32]. In our study, we individually knocked down YTHDF1/2/3 and IGF2BP1/2/3 in two NPC cell lines and observed that only knockdown of IGF2BP2 significantly inhibited the protein level of ANKRD22 (Fig. 5A and Supplementary Fig. 5A). Furthermore, knockdown of IGF2BP2 also decreased the level of ANKRD22 mRNA (Fig. 5B). RIP RT-qPCR confirmed the binding between IGF2BP2 protein and ANKRD22 mRNA (Fig. 5C). Additionally, after inhibition of METTL14, the enrichment of ANKRD22 mRNA by anti-IGF2BP2 specific antibody was significantly impaired, while overexpression of METTL14 significantly increased this binding efficiency (Fig. 5D). IF and nuclear-cytoplasmic fractionation assays showed that IGF2BP2 was mainly localized in the cytoplasm (Supplementary Fig. 5B-C). These findings suggest that IGF2BP2 may serve as an m^{6}A reader for METTL14-mediated ANKRD22 m^{6}A modification.

We subsequently treated the cells with actinomycin D. The degradation of ANKRD22 mRNA was significantly accelerated in IGF2BP2 knockdown NPC cells compared with control cells (Fig. 5E), which inhibited the effect of METTL14 overexpression on the degradation rate of ANKRD22 mRNA (Fig. 5F). Polysome analysis in cells with IGF2BP2 knockdown showed a significant reduction of ANKRD22 mRNA in the translation pool, while β-actin mRNA remained unchanged (Fig. 5G and Supplementary Fig. 5D), indicating that IGF2BP2 promotes the translation of ANKRD22 mRNA. To understand the potential mechanism by which IGF2BP2 promotes ANKRD22 mRNA translation, we performed immunoprecipitation (IP) and found that IGF2BP2 physically interacted with eukaryotic initiation factors such as eIF4E, eIF4G, and eIF3A (Fig. 5H). On the other hand, RIP RT-qPCR results showed that knockdown of IGF2BP2 significantly inhibited the binding of eIF4E, eIF4G, and eIF3A to ANKRD22 mRNA (Fig. 5I and Supplementary Fig. 5E). These results suggest that IGF2BP2 may recruit eukaryotic initiation factors to ANKRD22 mRNA to enhance its translation. Furthermore, luciferase reporter assays revealed that knockdown of IGF2BP2 reduced the luciferase activity from the wild-type ANKRD22 5' UTR, while it had no effect on the luciferase activity from the m^{6}A mutant of ANKRD22 5' UTR (Supplementary Fig. 5F). These data indicate that IGF2BP2 enhances the stability and translation of ANKRD22 mRNA by recognizing the m^{6}A site on ANKRD22 mRNA. Moreover, knockdown of IGF2BP2 attenuated the effects of METTL14 on the levels of ANKRD22 mRNA (Supplementary Fig. 5G), protein (Fig. 5J), and the luciferase activity from ANKRD22 5' UTR (Fig. 5K). Altogether, these findings suggest that IGF2BP2 enhances the stability and translational efficiency of ANKRD22 mRNA by recognizing and binding to the METTL14-mediated m^{6}A modification site on ANKRD22 mRNA.

METTL14 prompts lipid metabolism in NPC cells by upregulating ANKRD22 expression

ANKRD22, a protein featuring four ankyrin repeat (ANKR) motifs, has been implicated in the development of various cancers [33–35]. Studies have suggested that ANKRD22 is localized to mitochondria and may be associated with lipid metabolism reprogramming [36]. Utilizing the GEO database GSE12452 dataset, we performed gene set enrichment analysis (GSEA) and observed a positive correlation between ANKRD22 expression in NPC and the expression of genes related to lipid metabolism (Supplementary Fig. 6A-F). Western blotting analysis of cytoplasmic and mitochondrial fractions isolated from NPC cells further substantiated that ANKRD22 was predominantly localized to mitochondria (Supplementary Fig. 7A). IF assays demonstrated the co-localization of ANKRD22 with mitochondria (Fig. 6A). Flow cytometry and IF assays revealed that overexpression of ANKRD22 increased the lipid content in cells (Fig. 6B and Supplementary Fig. 7B-C) and counteracted the effect of METTL14 knockdown on lipid content in NPC cells (Fig. 6C and Supplementary Fig. 7D). Conversely, knockdown of ANKRD22 reduced the lipid content in NPC cells (Fig. 6B and Supplementary Fig. 7B-C) and mitigated the effect of METTL14 overexpression on lipid content (Fig. 6C and Supplementary Fig. 7E). These results suggest that METTL14 may promote lipid metabolism in NPC cells by upregulating ANKRD22.

The ANKR motif within ANKRD22 is known for its specific mediation of protein-protein interactions [37]. To further explore the mechanism through which ANKRD22 promotes lipid metabolism in NPC cells, we investigated whether ANKRD22 interacts with key enzymes on the mitochondria to facilitate lipid synthesis. The mitochondrial citrate/isocitrate carrier (CIC) SLC25A1 plays a pivotal role in exporting citrate from the mitochondria to the cytoplasm, thereby promoting de novo lipogenesis [38, 39]. Co- IP assays revealed the interaction between ANKRD22 and SLC25A1 (Fig. 6D and Supplementary Fig. 7F). IF assays further demonstrated the co-localization of SLC25A1 and ANKRD22 proteins on mitochondrial (Fig. 6E). Moreover, IP assays showed that METTL14 promotes the binding of ANKRD22 to SLC25A1 (Fig. 6F). Overexpression of ANKRD22 increased the cytoplasmic citrate content (Fig. 6G), and the addition of the SLC25A1-specific inhibitor compound CTPI-2 reversed the effect of ANKRD22 on citrate content (Fig. 6G). Citrate serves as a source of acetyl-CoA for fatty acid synthesis in the cytoplasm. Of note, overexpression of ANKRD22 increased the levels of acetyl-CoA in CNE2 and HONE1 cells (Fig. 6H) and mitigated the effect of siMETTL14 on cytoplasmic acetyl-CoA levels (Fig. 6I). Conversely, knockdown of ANKRD22 decreased the abundance of acetyl-CoA in cells (Fig. 6H) and attenuated the effect of METTL14 overexpression on cellular acetyl-CoA content (Fig. 6I). These findings indicate that ANKRD22, through its interaction with SLC25A1, mediates the impact of METTL14 on lipid metabolism in NPC cells.

ANKRD22 activates downstream gene transcription through enhancing H3K27AC

Acetyl-CoA serves as a central metabolic intermediate, acting as a key precursor for lipid production and the sole donor of acetyl groups for intracellular histone acetylation [40, 41]. Histone acetylation, exemplified by histone H3 lysine 27 acetylation (H3K27AC), is a well-established marker of active chromatin associated with gene expression [42, 43]. Analysis of the gene microarray dataset GSE12452 identified two molecules related to the cell skeleton, PLEK2 and FERMT1, as well as two cell cycle-related molecules, GINS3 and POLE2, displaying strong correlations with ANKRD22 (Supplementary Fig. 8A-B and Supplementary Table 8). These four proteins exhibited elevated expression in NPC tissues (Supplementary Fig. 8C). Chromatin immunoprecipitation (ChIP)-seq data for H3K27AC in NPC cell lines (C666-1, HK1, and HNE1) from the ENCODE database [44] (visualized through the UCSC browser) demonstrated high H3K27AC signals at the GINS3, POLE2, PLEK2, and FERMT1 genes (Supplementary Fig. 9), suggesting the importance of H3K27AC in driving the expression of these genes and promoting invasion, migration, and proliferation in NPC. Additionally, the promoter region of METTL14 was also enriched with H3K27AC signals (Supplementary Fig. 9), potentially contributing to its high expression in NPC. Treatment of cells with the histone acetyltransferase inhibitor C646 significantly reduced H3K27AC (Fig. 7A) and led to a significant decrease in the RNA levels of GINS3, POLE2, PLEK2, FERMT1, and METTL14 (Supplementary Fig. 8D) as well as their protein levels (Fig. 7A). Overexpression of ANKRD22 enhanced H3K27AC in cells (Fig. 7B) and upregulated the RNA and protein levels of GINS3, POLE2, PLEK2, FERMT1, and METTL14 (Supplementary Fig. 8E and Fig. 7B). Notably, these effects were reversed when C646 was added (Fig. 7C-D). Furthermore, ChIP-qPCR assays confirmed that overexpression of ANKRD22 enhanced H3K27AC near the promoters of these genes (Supplementary Fig. 8F), while adding C646 attenuated the effect of ANKRD22 on H3K27AC of these genes (Fig. 7E). These results demonstrate that the heightened H3K27AC signal induced by ANKRD22 overexpression can, on one hand, promote the increased expression of cytoskeleton-related proteins (PLEK2, FERMT1) and cell cycle-related proteins (GINS3, POLE2), thereby enhancing the invasion, migration and proliferation of NPC cells. On the other hand, it can also promote the transcription of METTL14, forming a feedback loop.

Positive correlations between METTL14 and ANKRD22 along with its downstream genes in NPC clinical samples

To further elucidate the role of METTL14 in promoting the malignant progression of NPC, we assessed the expression of molecules such as ANKRD22, GINS3, POLE2, PLEK2, FERMT1, and METTL14 in subcutaneous tumors (Supplementary Fig. 10A) and lung metastatic tissues (Supplementary Fig. 10B). IHC data showed heightened expression levels of ANKRD22, GINS3, POLE2, PLEK2, and FERMT1 in the METTL14 overexpression group and diminished expression levels in the METTL14 knockdown group. Further validation was performed through IHC analysis on paraffin sections of 70 NPC and 40 adjacent non-tumor NPE tissues (Fig. 8A-B). In comparison to NPE tissues, the levels of METTL14, ANKRD22, GINS3, POLE2, PLEK2, and FERMT1 were upregulated in NPC tissues. Moreover, the expression of METTL14 was significantly positively correlated with the expression of ANKRD22, GINS3, POLE2, PLEK2, and FERMT1 (Fig. 8C). These findings underscore the crucial role of METTL14 in promoting the malignant progression of NPC.

Discussion

This study unveils the pivotal role of METTL14-mediated m^6A modification in the progression of NPC. METTL14 facilitates the expression of ANKRD22 through the METTL14-IGF2BP2-ANKRD22 signaling axis. ANKRD22, in turn, interacts with the citrate transporter protein SLC25A1, elevating intracellular acetyl-CoA levels. This increase promotes lipid synthesis in NPC cells, sustaining rapid proliferation and metastasis of cancer cells. Simultaneously, heightened acetyl-CoA levels regulate epigenetic modifications, inducing high H3K27AC signals near the promoters of cell cycle and cytoskeleton-related genes, thereby accelerating the proliferation and metastasis of NPC. Notably, we observed that elevated acetyl-CoA levels also enhance H3K27AC near the promoter of METTL14, leading to an upregulation of METTL14 expression, thus forming a positive feedback loop (Fig. 8D). This feedback loop further perpetuates the proliferation and metastasis of NPC.

Alterations in epigenetic modifications, encompassing DNA, histone, and RNA modifications, are pivotal contributors to the dysregulation of gene expression and play crucial roles in tumorigenesis. In recent years, the significance of RNA modifications in cancer has garnered attention, with the discovery of over 100 types of RNA modifications[45]. Among these modifications, m^6A modification stands out as the most abundant and highly conserved modification on transcripts, characterized by the consensus sequence [G/A/U] [G > A] m^6A C [U > A > C] [46, 47]. It is prevalent in non-coding regions such as the 5' UTR [48, 49] and 3' UTR [50, 51], as well as in the coding sequence (CDS) [52, 53]. The m^6A modification is dynamically regulated by methyltransferase writers, demethylase erasers, and subsequently recognized by readers. This intricate process determines the fate of numerous RNA molecules, thereby influencing dysregulated gene expression and impacting tumor progression [54–56].

METTL14, a key component of the m^{6}A methyltransferase complex, has been implicated in various cancers, exerting a significant role in tumor progression. For instance, in pancreatic cancer, METTL14 is upregulated, leading to decreased PERP levels through the m^{6}A-YTHDF2 axis, thereby promoting cancer growth and metastasis [57]. In osteosarcoma (OS), METTL14, highly expressed, prevents the degradation and enhances the translational efficiency of MN1 mRNA through the m^{6}A-IGF2BP2 axis, contributing to tumorigenicity and conferring all-trans-retinoic acid resistance [58]. While prior studies have reported that m^{6}A modification levels mediated by the methyltransferases WTAP and METTL3 can promote NPC development [26–28], the specific biological role and regulatory mechanism of METTL14 in NPC have not been elucidated to date. In this study, we observed a significant upregulation of METTL14 expression in NPC tissues, closely associated with poor prognosis in patients. Additionally, m^{6}A dot blot assays revealed an overall increase in RNA m^{6}A levels in NPC tissues compared to nasopharyngeal chronic inflammation tissues. Through in vitro and in vivo experiments, we demonstrated that METTL14 promotes the proliferation and metastasis of NPC cells, indicating a close association between METTL14 expression and the progression of NPC. Leveraging the analysis of m^{6}A and gene expression profiling microarray data [29], we identified candidate genes and confirmed in NPC cells that METTL14 positively regulated the RNA and protein levels of ANKRD22. Moreover, our findings indicate that METTL14 upregulates ANKRD22 expression, thereby promoting the malignant progression of NPC, establishing ANKRD22 as a crucial target gene of METTL14.

ANKRD22, situated on chromosome 10q23.31, is a protein featuring four ANKR motifs and has been implicated in the development of various tumors [33, 34, 36, 59, 60]. Despite its reported involvement in tumorigenesis, the role of ANKRD22 in NPC remains unexplored. Our investigation unveiled that ANKRD22 plays a crucial role in promoting the proliferation, migration, and invasion of NPC cells. Furthermore, as ANKRD22 is localized in the mitochondria [36], it implies a potential association with tumor metabolism. However, the regulatory mechanisms and functions of ANKRD22 in tumor cell metabolism reprogramming during tumorigenesis remain poorly understood. Our data analysis revealed a robust enrichment of gene sets associated with lipid metabolism reprogramming in NPC samples exhibiting high ANKRD22 expression. Experimental evidence further affirmed that the overexpression of ANKRD22 facilitates lipid metabolism reprogramming, augmenting cellular lipid content. These findings suggest that ANKRD22 influences the proliferation and metastasis of NPC cells through metabolic reprogramming. Notably, ANKRD22 also counteracted the reduction in lipid content in NPC cells mediated by METTL14 knockdown, indicating that METTL14 upregulates ANKRD22 expression to promote lipid metabolism in NPC cells.

Lipid metabolism reprogramming has emerged as a hallmark feature of cancer cells, playing a pivotal role in cancer progression. Lipids serve as essential components for cell membrane formation during rapid proliferation and act as an energy source, contributing to growth and metastasis. Cancer cells primarily obtain lipids through de novo synthesis and exogenous uptake. Previous studies have demonstrated the upregulation of enzymes involved in both fatty acid synthesis and catabolism, along with lipid accumulation, in various cancer types [61, 62]. In lung adenocarcinoma, downregulation of fatty acid synthase ACLY reduced both proliferation and metastasis [63]. In hepatocellular carcinoma, hepatic mTORC2 promoted de novo lipid synthesis, resulting in lipid deposition and tumor development [64]. The mitochondrial citrate/isocitrate carrier (CIC) SLC25A1 plays a critical role by exporting citrate from the mitochondria to the cytoplasm. This action upregulates acetyl-CoA synthesis, facilitating de novo lipid synthesis [38, 39]. Acetyl-CoA serves as a substrate not only for lipid synthesis but also for histone acetylation, a modification that promotes open chromatin conformation and enhances the expression of oncogenes, thereby fostering cancer growth and metastasis [65]. Our study uncovered that the mitochondrial protein ANKRD22 interacts with SLC25A1, enhancing its citrate transport activity. This interaction leads to increased acetyl-CoA levels and elevated H3K27 acetylation (H3K27AC). Importantly, the heightened H3K27AC levels upregulate the expression of cell cycle-related genes (GINS3 and POLE2) and cytoskeleton-related genes (PLEK2 and FERMT1), thereby promoting the proliferation, migration, and invasion of NPC cells. Notably, the positive correlation between the expression of METTL14 and ANKRD22, GINS3, POLE2, PLEK2, and FERMT1 in NPC tissues underscores the clinical significance of the METTL14-ANKRD22 axis in driving the growth and metastasis of NPC.

The analysis of clinical tissue samples from NPC revealed a substantial increase in both the RNA and protein levels of ANKRD22. To understand the impact of m^{6}A modification on ANKRD22 expression, we explored two prominent m^{6}A reader families, namely YTHDF1/2/3 and IGF2BP1/2/3 [30–32]. Our investigation uncovered that the depletion of IGF2BP2 significantly diminished both the RNA and protein levels of ANKRD22. Moreover, the absence of IGF2BP2 resulted in decreased stability and translation efficiency of ANKRD22 mRNA. This suggests that IGF2BP2 serves as a reader for METTL14-mediated m^{6}A modification on ANKRD22, thereby enhancing the stability and translation efficiency of ANKRD22 mRNA and contributing to its upregulation in NPC tissues.

Significantly, we observed heightened H3K27AC signals near the METTL14 promoter. Our data confirmed that the augmented H3K27AC, resulting from increased acetyl-CoA content mediated by ANKRD22, facilitated METTL14 expression. This suggests the establishment of a positive feedback loop, METTL14-m^{6}A-ANKRD22, potentially contributing to the elevated expression of METTL14 and high m^{6}A levels in NPC. In our analysis of m^{6}A and gene expression profiling microarray data [29], we verified ANKRD22 as a crucial target of METTL14. However, other genes also exhibited substantial upregulation in both m^{6}A modification status and mRNA expression in NPC tissues (Hyper-up). This implies that there might be additional molecules regulated by METTL14-mediated m^{6}A modification, impacting NPC development, warranting further investigation. Additionally, our findings indicate that METTL14 promotes lipid metabolism in NPC cells through ANKRD22 upregulation. Developing METTL14-based inhibitors targeting ANKRD22 to impede lipid metabolism in tumor cells emerges as a promising strategy for future NPC treatment.

In summary, our findings elucidate a molecular mechanism wherein METTL14 facilitates lipid metabolism in NPC cells by elevating ANKRD22, establishing an aberrant regulatory loop that sustains m^{6}A modifications in NPC cells. ANKRD22, through its impact on cellular lipid metabolism, raises intracellular acetyl-CoA levels, enhances downstream H3K27AC gene expression, and ultimately contributes to tumorigenesis. This study expands our comprehension of METTL14's role in NPC development, offering insights that can guide future research and exploration of therapeutic strategies for NPC.

Methods

NPC clinical samples

The clinical samples in this study encompassed various tissue types, including fresh NPC tissues, control tissues from chronic nasopharyngeal inflammation, and paraffin-embedded NPC tissues. For RNA extraction and reverse transcription quantitative real-time polymerase chain reaction (RT-qPCR), we utilized 28 fresh NPC tissues and 7 chronic nasopharyngeal inflammation tissues obtained from Xiangya Hospital of Central South University (Supplementary Table 1). Paraffin-embedded tissue sections, comprising 80 NPC tissues and 42 adjacent non-tumor nasopharyngeal epithelial (NPE) tissues with clinical prognostic information (Supplementary Table 2), were sourced from the Affiliated Cancer Hospital of Xiangya School of Medicine, Central South University. These sections were employed for immunohistochemistry (IHC) to investigate the correlation between METTL14 and ANKRD22 expression and patient prognosis. Furthermore, an additional set of paraffin-embedded tissue sections, consisting of 70 NPC tissues and 40 adjacent non-tumor NPE tissues (Supplementary Table 3), obtained from Xiangya Hospital of Central South University, were used for IHC analysis to explore the correlation between the expression of METTL14, ANKRD22, GINS3, POLE2, PLEK2 and FERMT1. All NPC clinical samples were confirmed by histopathological examination. This study was approved by the Joint Ethics Committee of the Central South University and informed consents were obtained from all participants.

Cell culture, plasmids, small interfering RNAs, and transfection

NPC cell lines (CNE2, HONE1) were maintained at the Institute of Cancer Research, Central South University. All NPC cells were cultured in RPMI-1640 medium (Life Technologies, NY, USA) supplemented with 10% fetal bovine serum (Gibco, MA, USA) and maintained in a humidified incubator at 37°C with 5% CO_2.

The METTL14-Flag overexpression plasmid was purchased from Addgene (Addgene, MA, USA). The ANKRD22-Flag overexpression plasmid was purchased from YouBio (YouBio, Changsha, China). The pMIR-Luciferase-Reporter plasmids with insertion of ANKRD22 5'UTR wild-type and mutant sequences were purchased from Tsingke (Tsingke, Beijing, China). All constructs were confirmed by sequencing. The siRNAs targeting METTL14, ANKRD22, IGF2BP1/2/3, and YTHDF1/2/3 were purchased from RiboBio (RiboBio, Guangzhou, China) and their sequences are listed in Supplementary Table 4. Plasmids were transfected with Lipofectamine 3000 (Life Technologies, NY, USA), while siRNAs were transfected using Hiperfect (Qiagen, NRW, Germany). The SLC25A1 inhibitor CTPI-2 (MedChemExpress, NJ, USA) was diluted to a concentration of 50 μM for cell treatment. The histone acetyltransferase inhibitor C646 (Selleck, Shanghai, China) was diluted to a concentration of 20 μM for cell treatment.

RT-qPCR

RNA was reverse transcribed into cDNA using the HiScript cDNA Synthesis Kit (Vazyme, Nanjing, China). SYBR Green (Bimake, TX, USA) was used for RT-qPCR analysis. β-actin was used as an internal reference. The primer sequences used are listed in Supplementary Table 5.

Western blotting

Cellular proteins were extracted using RIPA buffer (Beyotime, Shanghai, China) with a protease inhibitor cocktail (Roche Applied Sciences, BW, Germany). Protein samples were separated by SDS-PAGE (8%-12%) and then transferred onto 0.2 μm PVDF membranes (Millipore, MA, USA). Membranes were then blocked with 5% skim milk at room temperature for 1 hour, followed by overnight incubation at 4°C with primary antibodies. After washing with phosphate-buffered saline supplemented with 0.1% Tween 20 (PBST), membranes were incubated with corresponding secondary antibodies at room temperature for 2 hours. Protein bands were detected using an ECL detection system (Millipore, MA, USA). β-tubulin was used as a loading control. The antibodies used are listed in Supplementary Table 6.

Immunohistochemistry

Paraffin-embedded sections of clinical NPC tissues and mouse xenograft tissues were subjected to immunohistochemistry (IHC) using the UltraSensitive™ SP (Mouse/Rabbit) IHC kit (MXB, Fujian, China). Staining was scored according to the intensity of staining and the percentage of stained cells. Intensity was assessed as none (0), faint (1), moderate (2), and strong (3); and the percentage of stained cells was assessed as none (0), ≤ 25% (1), 25–50% (2), 50–75% (3), and > 75% (4). The final score was calculated as the product of the intensity score and the percentage score. Two professional pathologists independently evaluated the stained sections. The antibodies used are listed in Supplementary Table 6.

Immunofluorescence (IF)

For mitochondrial staining, pre-warmed medium containing 200 nM Mito-Tracker Red CMXRos (Beyotime, Shanghai, China) at 37°C was added to NPC cells and incubated at 37°C for 30 min. Cells were fixed with 4% paraformaldehyde pre-warmed at 37°C, and the membranes were penetrated with 0.25% Triton X-100 and then blocked with 5% BSA. Overnight incubation with primary antibodies was performed at 4°C, followed by incubation with corresponding fluorescently labeled secondary antibodies at 37°C for 1 hour. Cell nuclei was counterstained with DAPI (Beyotime, Shanghai, China) and images were captured using a laser confocal microscope (Leica, HE, Germany). The antibodies used are listed in Supplementary Table 6.

Wound healing and transwell assays

For the wound healing assay, sterile 10 μl pipette tips were used to create uniform scratches on transfected cells in a 6-well plate. Images were captured under a microscope at 0 hour and 24 hours, respectively.

For the transwell invasion and migration assay, cells suspended in RPMI-1640 medium were added to the upper chamber of a transwell insert with or without 10% Matrigel (BD, Shanghai, China), while RPMI-1640 medium containing 20% FBS was added to the bottom chamber. Cells located on the lower surface of the upper chamber were fixed with 4% paraformaldehyde, stained with 1% crystal violet, and observed under an inverted phase-contrast microscope.

MTT and colony formation assays

For the MTT assay, 1000 transfected cells were seeded into each well of a 96-well plate. After cell adhesion, 20 μl MTT (Beyotime, Shanghai, China) was added to each well and incubated at 37°C for 4 hours. Subsequently, the culture medium was removed, and 200 μl of DMSO was added. The absorbance was measured at 490 nm on a microplate reader.

For the colony formation assay, 2000 transfected cells were seeded in a 12-well plate and cultured for 7 days. The cells were then fixed with 4% paraformaldehyde and stained with 0.1% crystal violet for analysis.

RNA m^6A dot blot

Briefly, the extracted total RNA was denatured at 65°C for 5 minutes and then mixed with SSC buffer. The RNA samples were then tranfered onto an Amersham Hybond-N + membrane (Solarbio, Beijing, China). The membranes were UV crosslinked for 5 minutes, then stained with 0.02% methylene blue (Coolaber, Beijing, China) and scanned for imaging as a loading control. Alternatively, the UV-crosslinked membranes were blocked with 5% skim milk in PBST for 1 hour and incubated overnight at 4°C with anti-m^6A antibody. After incubation with the secondary antibody, dot blot signals were visualized using an imaging system. The antibodies used are listed in Supplementary Table 6.

Animal experiments

Female BALB/C nude mice were randomly divided into four groups, with six mice in each group. A total of 2×10^6 CNE2 cells transfected with empty vector, METTL14 overexpression vector, negative control (NC), or METTL14 siRNA were injected subcutaneously or via the tail vein, respectively. For the subcutaneous tumor model, tumor growth was monitored every 5 days and tumor size was assessed by calculating the tumor volume V = 1/2 x (length) x (width) x (width). Thirty days after subcutaneous inoculation, mice were sacrificed by cervical dislocation and the tumor tissue was excised. The tumor masses were then weighed. For the tail vein lung metastasis model, mice were sacrificed by cervical dislocation 30 days after inoculation, lung tissue was removed, and the number of metastatic nodules on the lung surface of each mouse was recorded to assess tumor metastasis. All animal studies were approved by the Institutional Laboratory of Animal Care and Use Committee at Central South University.

Hematoxylin-Eosin staining (H&E)

Paraffin-embedded mouse tissue sections were heated at 65°C for 2 h. After dewaxed with xylene and hydrated with gradient ethanol, the nuclei were stained with hematoxylin solution (Biosharp, Anhui, China) and then the cytoplasm was stained with eosin solution (Biosharp, Anhui, China). Finally, the sections were sealed and preserved with neutral resin.

Actinomycin D treatment

Actinomycin D (Abmole, TX, USA) was added to NPC cells at a final concentration of 5 μg/ml, and RNA was collected for RT-qPCR at 0 hour, 2 hours, and 4 hours. The primers used are listed in Supplementary Table 5.

Polysome analysis

Cells in dishes were incubated with 100 μg/ml cycloheximide (Beyotime, Shanghai, China) for 5 min at 37°C and 5% CO_2 in a humidified incubator. Subsequently, cells were collected by gentle scraping and centrifugation after washing the cells twice with pre-cooled PBS containing 100 μg/ml cycloheximide. The cells were resuspended by adding hypotonic buffer (5 mM Tris-HCl pH 7.5, 15 mM KCl, 25 mM $MgCl_2$, 1 × protease inhibitor) supplemented with 100 μg/ml cycloheximide, 0.5% Triton X-100, 0.5% sodium deoxycholate, 100 U RNase inhibitor, and 2 mM DTT. Following centrifugation, the supernatant was extracted. Ten percent of the supernatant, representing the input, was retained, while the remaining portion was transferred to tubes of an ultracentrifuge with a sucrose gradient (5%, 10%, 25%, 35%, 50%) that had been allowed to stand overnight. The mixture was centrifuged at 32,000 rpm for 2 hours at 4°C. Subsequent to centrifugation, RNA from distinct ribosome fractions was extracted and subjected to analysis through RT-qPCR. The primers used are listed in Supplementary Table 5.

MeRIP RT-qPCR

Total RNA was extracted using TRIzol reagent (Invitrogen, Cali, USA). riboMeRIP™ m^6A Transcriptome Profiling Kit (RiboBio, Guangzhou, China) was then used following to the manufacturer's instructions. The RNA enriched by anti-m^6A antibody was purified and recovered by Magen Hipure Serum/plasma miRNA Kit (Magen, Shanghai, China), and analyzed by RT-qPCR. The primers used are listed in Supplementary Table 5.

RNA pull-down

ANKRD22 5'UTR-wt and 5'UTR-mut were transcribed in vitro using the Biotin RNA Labeling Mix kit (Roche, BS, Switzerland) and T7 RNA polymerase (Promega, WI, USA). The cell lysate was incubated with the biotin-labeled RNA at room temperature for 2 hours, followed by the addition of 50 μl Streptavidin Magnetic Beads (Invitrogen, Cali, USA) and incubation overnight at 4°C with rotation. Finally, the bound proteins were analyzed by western blotting.

Luciferase reporter assay

After 48 hours of cell transfection, the luciferase activity was assessed using the Dual-Luciferase Reporter Assay System (Promega, WI, USA) according to the manufacturer's instructions. Relative luciferase activity was obtained by normalizing with Renilla luciferase activity.

Lipid staining

Cells were stained with BODIPY 493/503 (GLPBIO, Cali, USA) for 15 min at 37°C protected from the light. The cells were counterstained with DAPI for 5 min and images were taken using a laser confocal microscope (Leica, HE, Germany). Alternatively, cells were collected for flow cytometry and data were analyzed using FlowJo v10 software (Treestar).

Measurement of citrate and acetyl-CoA

After 48 hours of cell transfection, the levels of citrate and acetyl-CoA were measured using the Mitochondrial Citrate Assay Kit (ZCIBIO, Shanghai, China) and the CheKine™ Acetyl-CoA Assay Kit (Abbkine, Wuhan, China), respectively, following the manufacturer's instructions.

Immunoprecipitation (IP)

Antibodies were mixed with 50 µl of protein A/G magnetic beads (Bimake, TX, USA) and incubated at room temperature for 2 hours with rotation, followed by the addition of cell lysates for overnight incubation at 4°C with rotation. After washing three times with GLB^+ buffer (10 mM NaCl, 10 mM Tris-HCl, 10 mM EDTA, 0.5% Triton-100), the enriched proteins were analyzed by western blotting. The antibodies used are listed in Supplementary Table 6.

RNA immunoprecipitation (RIP) and chromatin immunoprecipitation (ChIP)

According to the manufacturer's instructions, the Magna RIP™ kit (Millipore, MA, USA) was used for RIP to analyze the interaction between METTL14, IGF2BP2, and ANKRD22 mRNA, followed by RT-qPCR analysis. Additionally, the ChIP Assay Kit (Beyotime, Shanghai, China) was used for ChIP according to the manufacturer's instructions, followed by RT-qPCR analysis. The primers used are listed in Supplementary Table 5.

Statistical analysis

Statistical analysis was performed using GraphPad Prism 8.0 software. When comparing differences between two groups, Student's t-test was used. For comparisons involving more than two groups, one-way ANOVA was used. All data are presented as mean ± standard deviation (SD). $p < 0.05$ was considered statistically significant. *$p < 0.05$, **$p < 0.01$, ***$p < 0.001$, ****$p < 0.0001$.

Declarations

Acknowledgements

The authors acknowledge the BioRender (www.biorender.com), as fig. 8D in this article was created with BioRender platform. This study was funded by the National Natural Science Foundation of China (U21A20382), the Natural Science Foundation of Hunan Province (2023SK2004), and the Natural Science Foundation of Changsha (kh2301025).

Authors' contributions

L.Y.L. designed the project and completed most experiments. Q.L.T., J.S.G., D.W. performed some of the experiments. Y.Z.M., Y.M.W., Q.J.Y. collected tissue samples. L.Y.L. analyzed the data and wrote the manuscript. F.X., Q.J.L., C.G., F.Y.W., M.Z., B.X., Z.Y.Z., L.S., P.C., and W.X. revised the manuscript. L.S., P.C., and W.X. are responsible for research supervision and funding acquisition. All authors read and approved the final manuscript.

Competing interests

The authors declare no competing interest.

References

1. Chen, Y.P., et al., *Nasopharyngeal carcinoma*. Lancet, 2019. 394(10192): p. 64–80.
2. Zeng, Z., et al., *Regulation network and expression profiles of Epstein-Barr virus-encoded microRNAs and their potential target host genes in nasopharyngeal carcinomas*. Sci China Life Sci, 2014. 57(3): p. 315–326.
3. Chan, A.T., P.M. Teo, and P.J. Johnson, *Nasopharyngeal carcinoma*. Ann Oncol, 2002. 13(7): p. 1007–15.
4. Xiong, W., et al., *A susceptibility locus at chromosome 3p21 linked to familial nasopharyngeal carcinoma*. Cancer Res, 2004. 64(6): p. 1972–4.
5. Hildesheim, A. and C.P. Wang, *Genetic predisposition factors and nasopharyngeal carcinoma risk: a review of epidemiological association studies, 2000–2011: Rosetta Stone for NPC: genetics, viral infection, and other environmental factors*. Semin Cancer Biol, 2012. 22(2): p. 107–16.
6. Ho, J.H., *An epidemiologic and clinical study of nasopharyngeal carcinoma*. Int J Radiat Oncol Biol Phys, 1978. 4(3–4): p. 182–98.
7. Paiar, F., et al., *Role of chemotherapy in nasopharyngeal carcinoma*. Oncol Rev, 2012. 6(1): p. e1.
8. Liew, K., et al., *Parallel genome-wide RNAi screens identify lymphocyte-specific protein tyrosine kinase (LCK) as a targetable vulnerability of cell proliferation and chemoresistance in nasopharyngeal carcinoma*. Cancer Lett, 2021. 504: p. 81–90.
9. Wong, K.C.W., et al., *Nasopharyngeal carcinoma: an evolving paradigm*. Nat Rev Clin Oncol, 2021. 18(11): p. 679–695.
10. Wei, F., et al., *Trend analysis of cancer incidence and mortality in China*. Sci China Life Sci, 2017. 60(11): p. 1271–1275.
11. Liu, T., et al., *The m6A reader YTHDF1 promotes ovarian cancer progression via augmenting EIF3C translation*. Nucleic Acids Res, 2020. 48(7): p. 3816–3831.
12. Xu, Y., et al., *The N6-methyladenosine METTL3 regulates tumorigenesis and glycolysis by mediating m6A methylation of the tumor suppressor LATS1 in breast cancer*. J Exp Clin Cancer Res, 2023. 42(1): p. 10.
13. Chen, H., et al., *RNA N(6)-Methyladenosine Methyltransferase METTL3 Facilitates Colorectal Cancer by Activating the m(6)A-GLUT1-mTORC1 Axis and Is a Therapeutic Target*. Gastroenterology, 2021. 160(4): p. 1284–1300.e16.
14. Wei, C.M., A. Gershowitz, and B. Moss, *Methylated nucleotides block 5' terminus of HeLa cell messenger RNA*. Cell, 1975. 4(4): p. 379–86.
15. Vu, L.P., Y. Cheng, and M.G. Kharas, *The Biology of m(6)A RNA Methylation in Normal and Malignant Hematopoiesis*. Cancer Discov, 2019. 9(1): p. 25–33.

16. Tong, J., R.A. Flavell, and H.B. Li, *RNA m(6)A modification and its function in diseases*. Front Med, 2018. 12(4): p. 481–489.
17. Ping, X.L., et al., *Mammalian WTAP is a regulatory subunit of the RNA N6-methyladenosine methyltransferase*. Cell Res, 2014. 24(2): p. 177–89.
18. Jia, G., et al., *N6-methyladenosine in nuclear RNA is a major substrate of the obesity-associated FTO*. Nat Chem Biol, 2011. 7(12): p. 885–7.
19. Zheng, G., et al., *ALKBH5 is a mammalian RNA demethylase that impacts RNA metabolism and mouse fertility*. Mol Cell, 2013. 49(1): p. 18–29.
20. Dominissini, D., et al., *Topology of the human and mouse m6A RNA methylomes revealed by m6A-seq*. Nature, 2012. 485(7397): p. 201–6.
21. Xiao, W., et al., *Nuclear m(6)A Reader YTHDC1 Regulates mRNA Splicing*. Mol Cell, 2016. 61(4): p. 507–519.
22. Li, M., et al., *Ythdf2-mediated m(6)A mRNA clearance modulates neural development in mice*. Genome Biol, 2018. 19(1): p. 69.
23. Wang, X., et al., *N6-methyladenosine-dependent regulation of messenger RNA stability*. Nature, 2014. 505(7481): p. 117–20.
24. Shi, H., et al., *YTHDF3 facilitates translation and decay of N(6)-methyladenosine-modified RNA*. Cell Res, 2017. 27(3): p. 315–328.
25. Shi, H., et al., *m(6)A facilitates hippocampus-dependent learning and memory through YTHDF1*. Nature, 2018. 563(7730): p. 249–253.
26. Li, Z.X., et al., *WTAP-mediated m(6)A modification of lncRNA DIAPH1-AS1 enhances its stability to facilitate nasopharyngeal carcinoma growth and metastasis*. Cell Death Differ, 2022. 29(6): p. 1137–1151.
27. Wang, Y.Q., et al., *TEAD4 is a master regulator of high-risk nasopharyngeal carcinoma*. Sci Adv, 2023. 9(1): p. eadd0960.
28. Hu, X., et al., *METTL3-stabilized super enhancers-lncRNA SUCLG2-AS1 mediates the formation of a long-range chromatin loop between enhancers and promoters of SOX2 in metastasis and radiosensitivity of nasopharyngeal carcinoma*. Clin Transl Med, 2023. 13(9): p. e1361.
29. Wang, Y.M., et al., *N6-Methyladenosine RNA Modification Landscape in the Occurrence and Recurrence of Nasopharyngeal Carcinoma*. World J Oncol, 2022. 13(4): p. 205–215.
30. Liao, S., H. Sun, and C. Xu, *YTH Domain: A Family of N(6)-methyladenosine (m(6)A) Readers*. Genomics Proteomics Bioinformatics, 2018. 16(2): p. 99–107.
31. Huang, H., et al., *Recognition of RNA N(6)-methyladenosine by IGF2BP proteins enhances mRNA stability and translation*. Nat Cell Biol, 2018. 20(3): p. 285–295.
32. Zaccara, S. and S.R. Jaffrey, *A Unified Model for the Function of YTHDF Proteins in Regulating m(6)A-Modified mRNA*. Cell, 2020. 181(7): p. 1582–1595.e18.
33. Yin, J., et al., *ANKRD22 promotes progression of non-small cell lung cancer through transcriptional up-regulation of E2F1*. Sci Rep, 2017. 7(1): p. 4430.
34. Wu, Y., et al., *ANKRD22 enhances breast cancer cell malignancy by activating the Wnt/β-catenin pathway via modulating NuSAP1 expression*. Bosn J Basic Med Sci, 2021. 21(3): p. 294–304.
35. Liu, X., et al., *ANKRD22 promotes glioma proliferation, migration, invasion, and epithelial-mesenchymal transition by upregulating E2F1-mediated MELK expression*. J Neuropathol Exp Neurol, 2023.
36. Pan, T., et al., *ANKRD22, a novel tumor microenvironment-induced mitochondrial protein promotes metabolic reprogramming of colorectal cancer cells*. Theranostics, 2020. 10(2): p. 516–536.
37. Li, J., A. Mahajan, and M.D. Tsai, *Ankyrin repeat: a unique motif mediating protein-protein interactions*. Biochemistry, 2006. 45(51): p. 15168–78.
38. Palmieri, F., *Mitochondrial transporters of the SLC25 family and associated diseases: a review*. J Inherit Metab Dis, 2014. 37(4): p. 565–75.
39. Palmieri, F., *The mitochondrial transporter family SLC25: identification, properties and physiopathology*. Mol Aspects Med, 2013. 34(2–3): p. 465–84.
40. Shi, L. and B.P. Tu, *Acetyl-CoA and the regulation of metabolism: mechanisms and consequences*. Curr Opin Cell Biol, 2015. 33: p. 125–31.
41. Guertin, D.A. and K.E. Wellen, *Acetyl-CoA metabolism in cancer*. Nat Rev Cancer, 2023. 23(3): p. 156–172.
42. Chen, Q., et al., *Histone acetyltransferases CBP/p300 in tumorigenesis and CBP/p300 inhibitors as promising novel anticancer agents*. Theranostics, 2022. 12(11): p. 4935–4948.
43. Barnes, C.E., D.M. English, and S.M. Cowley, *Acetylation & Co: an expanding repertoire of histone acylations regulates chromatin and transcription.* Essays Biochem, 2019. 63(1): p. 97–107.
44. Rosenbloom, K.R., et al., *ENCODE whole-genome data in the UCSC Genome Browser: update 2012*. Nucleic Acids Res, 2012. 40(Database issue): p. D912-7.
45. Cantara, W.A., et al., *The RNA Modification Database, RNAMDB: 2011 update*. Nucleic Acids Res, 2011. 39(Database issue): p. D195-201.
46. Schibler, U., D.E. Kelley, and R.P. Perry, *Comparison of methylated sequences in messenger RNA and heterogeneous nuclear RNA from mouse L cells*. J Mol Biol, 1977. 115(4): p. 695–714.
47. Zhao, B.S., I.A. Roundtree, and C. He, *Post-transcriptional gene regulation by mRNA modifications*. Nat Rev Mol Cell Biol, 2017. 18(1): p. 31–42.
48. Meyer, K.D., et al., *5′ UTR m(6)A Promotes Cap-Independent Translation*. Cell, 2015. 163(4): p. 999–1010.
49. Li, Z., et al., *N(6)-methyladenosine regulates glycolysis of cancer cells through PDK4*. Nat Commun, 2020. 11(1): p. 2578.
50. Lan, T., et al., *KIAA1429 contributes to liver cancer progression through N6-methyladenosine-dependent post-transcriptional modification of GATA3*. Mol Cancer, 2019. 18(1): p. 186.
51. Ni, Z., et al., *JNK Signaling Promotes Bladder Cancer Immune Escape by Regulating METTL3-Mediated m6A Modification of PD-L1 mRNA*. Cancer Res, 2022. 82(9): p. 1789–1802.
52. Lin, X., et al., *RNA m(6)A methylation regulates the epithelial mesenchymal transition of cancer cells and translation of Snail.* Nat Commun, 2019. 10(1): p. 2065.
53. Li, T., et al., *METTL3 facilitates tumor progression via an m(6)A-IGF2BP2-dependent mechanism in colorectal carcinoma*. Mol Cancer, 2019. 18(1): p. 112.

54. Chen, S., et al., *Fusobacterium nucleatum reduces METTL3-mediated m(6)A modification and contributes to colorectal cancer metastasis*. Nat Commun, 2022. 13(1): p. 1248.
55. Shi, Y., et al., *YTHDF1 links hypoxia adaptation and non-small cell lung cancer progression*. Nat Commun, 2019. 10(1): p. 4892.
56. Zou, Y., et al., *N6-methyladenosine regulated FGFR4 attenuates ferroptotic cell death in recalcitrant HER2-positive breast cancer*. Nat Commun, 2022. 13(1): p. 2672.
57. Wang, M., et al., *Upregulation of METTL14 mediates the elevation of PERP mRNA N(6) adenosine methylation promoting the growth and metastasis of pancreatic cancer*. Mol Cancer, 2020. 19(1): p. 130.
58. Li, H.B., et al., *METTL14-mediated epitranscriptome modification of MN1 mRNA promote tumorigenicity and all-trans-retinoic acid resistance in osteosarcoma*. EBioMedicine, 2022. 82: p. 104142.
59. Chen, H., et al., *ANKRD22 is a potential novel target for reversing the immunosuppressive effects of PMN-MDSCs in ovarian cancer*. J Immunother Cancer, 2023. 11(2).
60. Qiu, Y., et al., *ANKRD22 is involved in the progression of prostate cancer*. Oncol Lett, 2019. 18(4): p. 4106–4113.
61. Menendez, J.A. and R. Lupu, *Fatty acid synthase and the lipogenic phenotype in cancer pathogenesis*. Nat Rev Cancer, 2007. 7(10): p. 763–77.
62. Koundouros, N. and G. Poulogiannis, *Reprogramming of fatty acid metabolism in cancer*. Br J Cancer, 2020. 122(1): p. 4–22.
63. Hatzivassiliou, G., et al., *ATP citrate lyase inhibition can suppress tumor cell growth*. Cancer Cell, 2005. 8(4): p. 311–21.
64. Guri, Y., et al., *mTORC2 Promotes Tumorigenesis via Lipid Synthesis*. Cancer Cell, 2017. 32(6): p. 807–823.e12.
65. He, W., Q. Li, and X. Li, *Acetyl-CoA regulates lipid metabolism and histone acetylation modification in cancer*. Biochim Biophys Acta Rev Cancer, 2023. 1878(1): p. 188837.

Figures

Fig.1

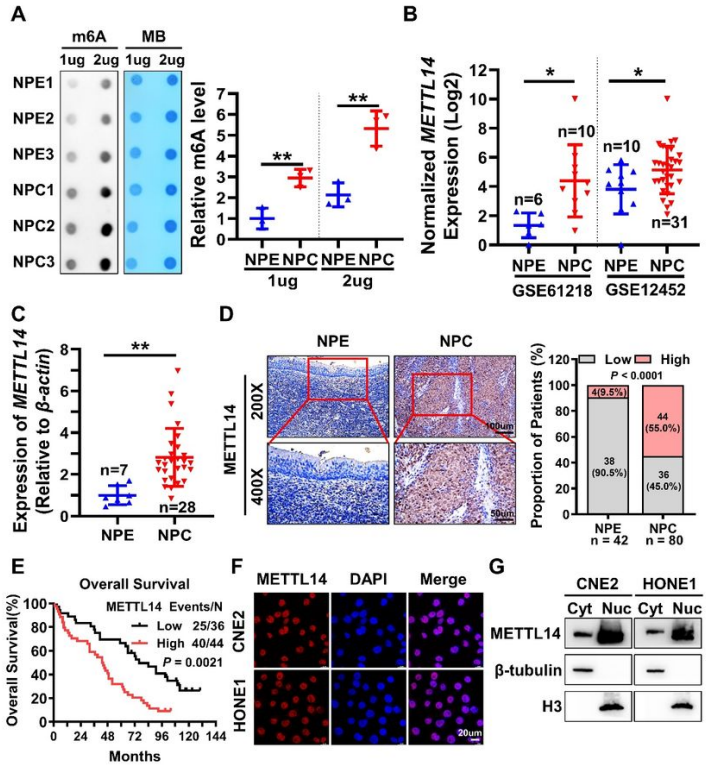

Figure 1

METTL14 is highly expressed in NPC and associated with poor prognosis of patients

A. RNA m^6A dot blot assays were employed to assess the m^6A levels of total RNA in 3 non-tumor NPE tissues and 3 NPC tissues (left panel), with grayscale scanning was conducted for statistical analysis (right panel). Methylene blue (MB) staining served as loading control.

B. METTL14 expression in NPC datasets GSE61218 and GSE12452.

C. METTL14 mRNA expression levels were detected in 28 NPC and 7 non-tumor NPE tissues by RT-qPCR.

D. IHC assays were applied to detect the expression of METTL14 protein in 80 NPC and 42 adjacent non-tumor NPE tissues. Scale bars: 200 ×, 100 μm; 400 ×, 50 μm. Left panel: representative images of METTL14 expression in NPC and NPE tissues. Right panel: statistical analysis of METTL14 expression in NPC and NPE tissues.

E. Kaplan-Meier overall survival (OS) was conducted for METTL14 expression in 80 patients with NPC.

F. IF assays were applied to detect the METTL14 localization in CNE2 and HONE1 cells. Cell nuclei were counterstained with DAPI (blue). Scale bar: 20 μm.

G. Protein nuclear-cytoplasmic fractionation assays were performed to assess the METTL14 localization in CNE2 and HONE1 cells. H3 was used as a nuclear marker, and β-tubulin was used as a cytoplasmic marker. Cyt: cytoplasm, Nuc: nucleus.

Data were presented as mean ± SD. *$p < 0.05$, ***$p < 0.001$.

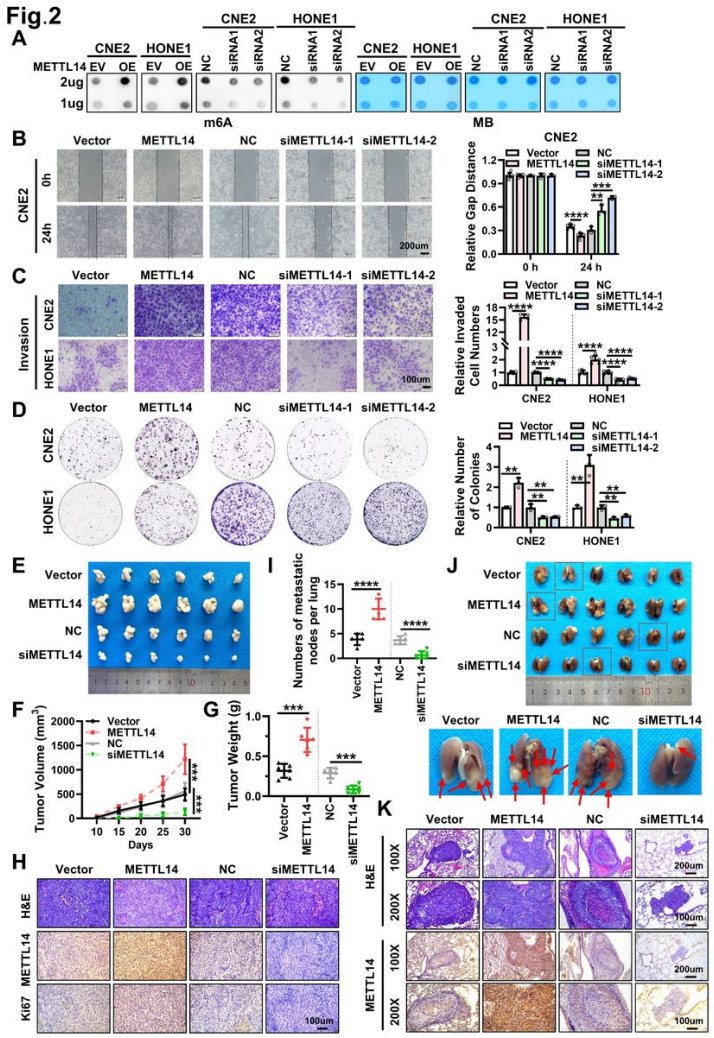

Figure 2

METTL14 promotes the proliferation and metastasis of NPC cells in vitro and in vivo

A. RNA m^6A dot blot assays were performed to detect the m^6A levels of total RNA after overexpression or knockdown of METTL14 in CNE2 and HONE1 cells. Methylene blue (MB) staining served as loading control.

B. Wound healing assays were used to assess cell migration after overexpression or knockdown of METTL14 in CNE2 cells. Representative images (left panel) and statistical analysis (right panel) were presented. Images were acquired at 0 and 24 hours. Scale bar: 200 μm.

C. Transwell invasion assays were performed to examine cell invasion ability after overexpression or knockdown of METTL14 in CNE2 and HONE1 cells. Representative images (left panel) and statistical analysis (right panel) were presented. Scale bar: 100 μm.

D. Colony formation assays were conducted to assess cell proliferation after overexpression or knockdown of METTL14 in CNE2 and HONE1 cells.

E. Images of subcutaneous tumors in nude mice (n = 6 per group).

F, G. Subcutaneous tumor volume growth curve (F) and tumor weight (G) in nude mice.

H. Representative images of subcutaneous tumor sections for H&E staining and IHC detection of METTL14 and Ki67 expression. Scale bar: 200 ×, 100 μm.

I. Quantification of the number of metastatic nodules on lung surface.

J. Representative images of lung tissue from nude mouse (upper panel, n = 6 per group). Arrows indicates metastatic nodules on the lung surface (lower panel).

K. Representative images of H&E-stained lung metastatic tumor foci and METTL14 expression by assayed IHC. Scale bars: 100 ×, 200 μm; 200 ×, 100 μm.

Data were presented as mean ± SD. $^{**}p < 0.01$, $^{***}p < 0.001$, $^{****}p < 0.0001$.

Fig.3

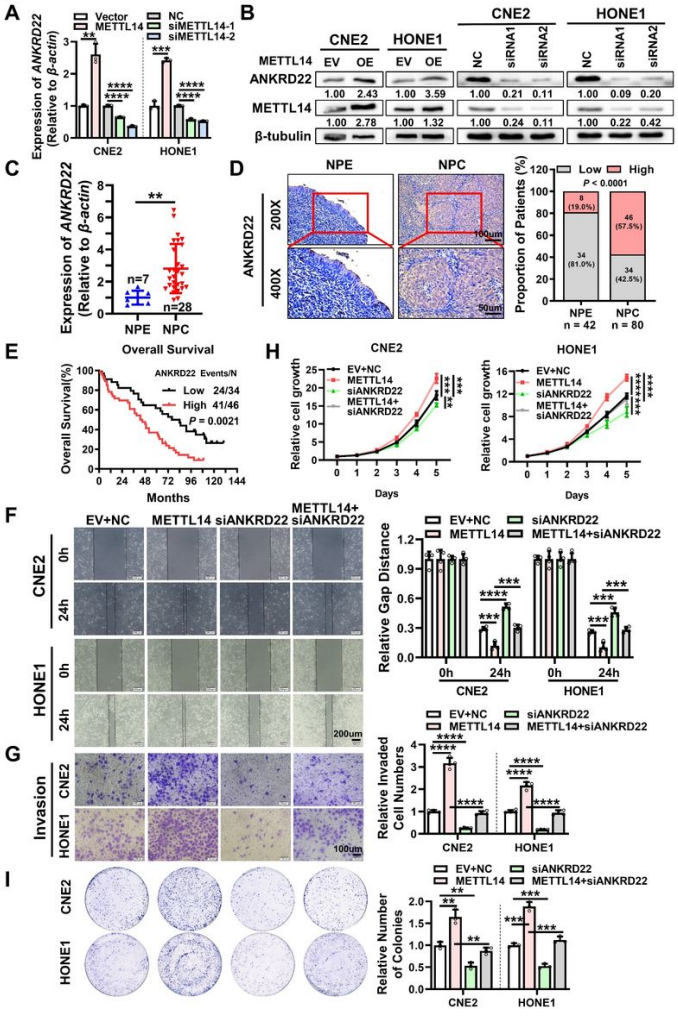

Figure 3

METTL14 upregulates the expression of ANKRD22 to promote NPC malignant progression

A, B. The mRNA (**A**) and protein (**B**) levels of ANKRD22 after overexpression or knockdown of METTL14 in CNE2 and HONE1 cells as detected by RT-qPCR and western blotting, respectively.

C.ANKRD22 mRNA expression levels in 28 NPC and 7 non-tumor NPE tissues quantified by RT-qPCR.

D. IHC assays were employed to determine the expression of ANKRD22 protein in 80 NPC and 42 adjacent non-tumor NPE tissues. Scale bars: 200 ×, 50 μm; 400 ×, 20 μm. Left panel: representative images of ANKRD22 expression in NPC and NPE tissues. Right panel: statistical analysis of ANKRD22 expression in

NPC and NPE tissues.

E. Kaplan-Meier overall survival (OS) was conducted for ANKRD22 expression in 80 patients with NPC.

F-I. Wound healing assays (**F**), Transwell invasion assays (**G**), MTT assays (**H**), and colony formations assays (**I**) were conducted to determine the effect of ANKRD22 on the METTL14-mediated migration, invasion, and proliferative of CNE2 and HONE1 cells. F, Scale bar: 200 μm. G, Scale bar: 100 μm.

Data were presented as mean ± SD. $^{**}p < 0.01$, $^{***}p < 0.001$, $^{****}p < 0.0001$.

Fig. 4

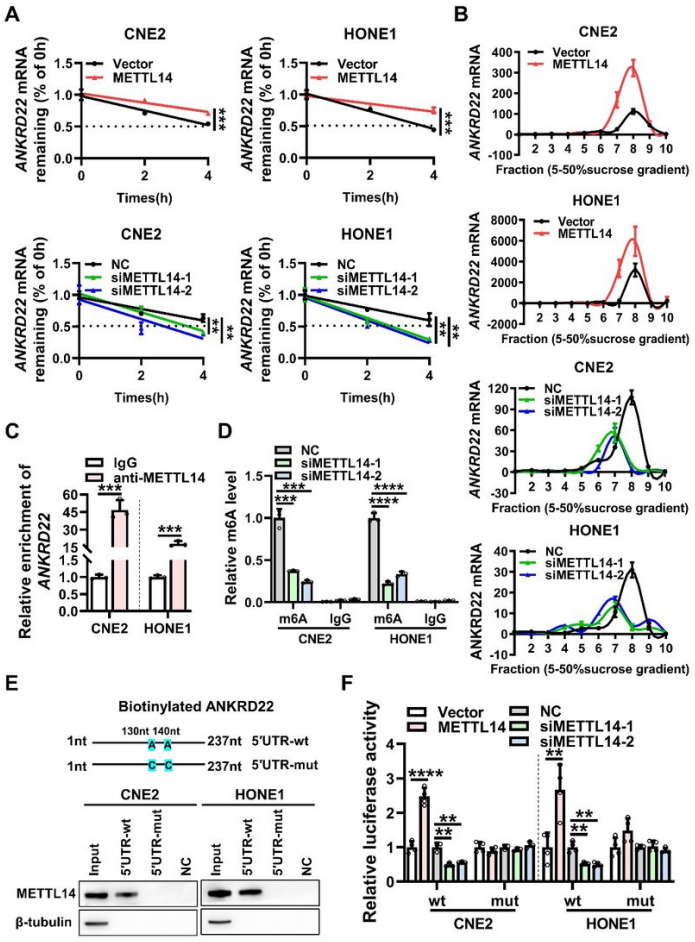

Figure 4

METTL14 enhances the stability and translation of ANKRD22 mRNA in an m^{6}A-dependent manner

A. The ANKRD22 mRNA stability in CNE2 and HONE1 cells overexpression of METTL14 (upper panel) or knockdown of METTL14 (lower panel) was examined after treatment with actinomycin D (5μg/ml) for the indicated times.

B. Polysome analysis was employed to determine the ANKRD22 mRNA translation efficiency after overexpression or knockdown of METTL14 in CNE2 and HONE1 cells. RNA from different ribosome fractions was extracted and analyzed by RT-qPCR.

C. RIP RT-qPCR assays were performed to assess the binding of ANKRD22 mRNA with METTL14 in CNE2 and HONE1 cells.

D. MeRIP RT-qPCR assays were conducted to assess the effect of knockdown of METTL14 on the m^{6}A level of ANKRD22 mRNA (66-175 nt) in CNE2 and HONE1 cells.

E. RNA pull-down assays were conducted to evaluate the interaction between METTL14 and ANKRD22 mRNA in CNE2 and HONE1 cells. NC: magnetic beads only.

F. Luciferase reporter assays were conducted to investigate the impact of METTL14 on the luciferase activity of the m^{6}A sequence within the ANKRD22 5'UTR in CNE2 and HONE1 cells.

Data were presented as mean ± SD. $^{**}p < 0.01$, $^{***}p < 0.001$, $^{****}p < 0.0001$.

Fig. 5

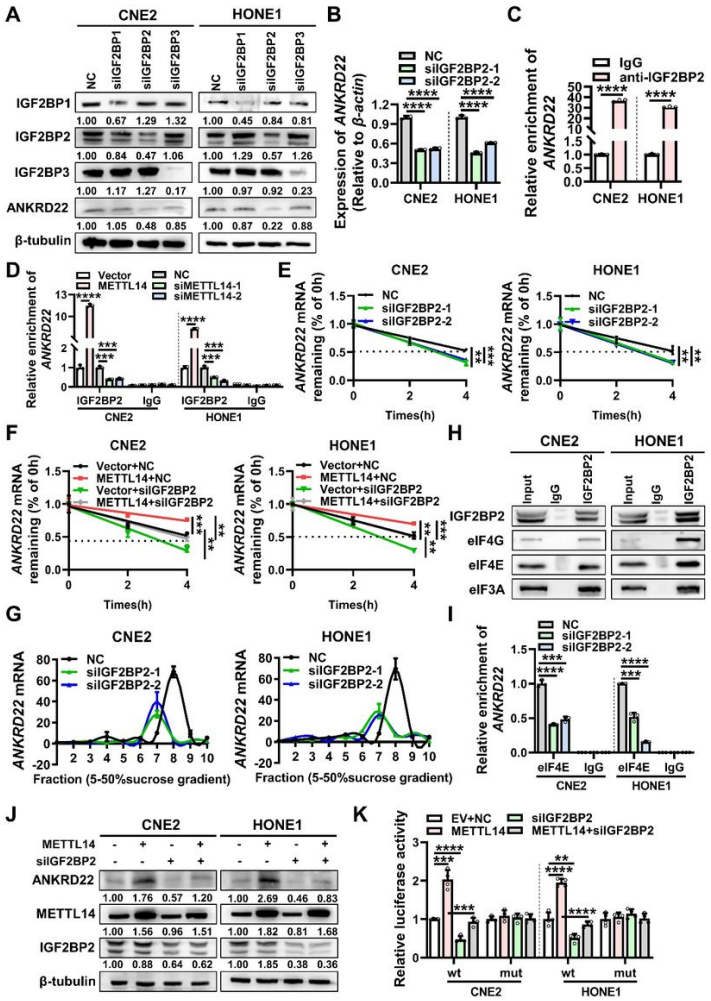

Figure 5

IGF2BP2 recognizes METTL14-mediated m^{6}A modification on ANKRD22 mRNA

A. Protein levels of ANKRD22 after knockdown of IGF2BP1/2/3 in CNE2 and HONE1 cells were detected by western blotting.

B. RT-qPCR assays were conducted to detect mRNA levels of ANKRD22 after knockdown of IGF2BP2 in CNE2 and HONE1 cells.

C. RIP RT-qPCR assays were conducted to assess ANKRD22 mRNA binding with IGF2BP2 in CNE2 and HONE1 cells.

D. RIP RT-qPCR assays were employed to assess IGF2BP2 binding to ANKRD22 mRNA after overexpression or knockdown of METTL14 in CNE2 and HONE1 cells.

E. After treatment of CNE2 and HONE1 cells with actinomycin D (5μg/ml) for the indicated times, the effect of knockdown of IGF2BP2 on ANKRD22 mRNA stability was examined in the cells.

F. After treatment of CNE2 and HONE1 cells with actinomycin D (5 μg/ml) for the indicated times, the effect of co-transfection of METTL14 overexpression vector and IGF2BP2 siRNA in cells on the stability of ANKRD22 mRNA was examined.

G. Polysome analysis was performed to assess the effect of knockdown of IGF2BP2 on the translation efficiency of ANKRD22 mRNA in CNE2 and HONE1 cells. RNAs in different ribosome fractions were extracted and analyzed by RT-qPCR.

H. IP assays were performed to analyze the binding of IGF2BP2 to eIF4G, eIF4E, and eIF3A in CNE2 and HONE1 cells.

I. RIP RT-qPCR assays were performed to assess the binding of eIF4E to ANKRD22 mRNA after knockdown of IGF2BP2 in CNE2 and HONE1 cells.

J. Protein levels of ANKRD22 after co-transfection of METTL14 overexpression vector and IGF2BP2 siRNA in CNE2 and HONE1 cells were detected by western blotting.

K. Luciferase reporter assays were employed to evaluate the luciferase activity of the m^6A sequence in the 5'UTR of ANKRD22 after co-transfection of METT14 overexpression vector and IGF2BP2 siRNA in CNE2 and HONE1 cells.

Data were presented as mean ± SD. $^{**}p < 0.01$, $^{***}p < 0.001$, $^{****}p < 0.0001$.

Fig. 6

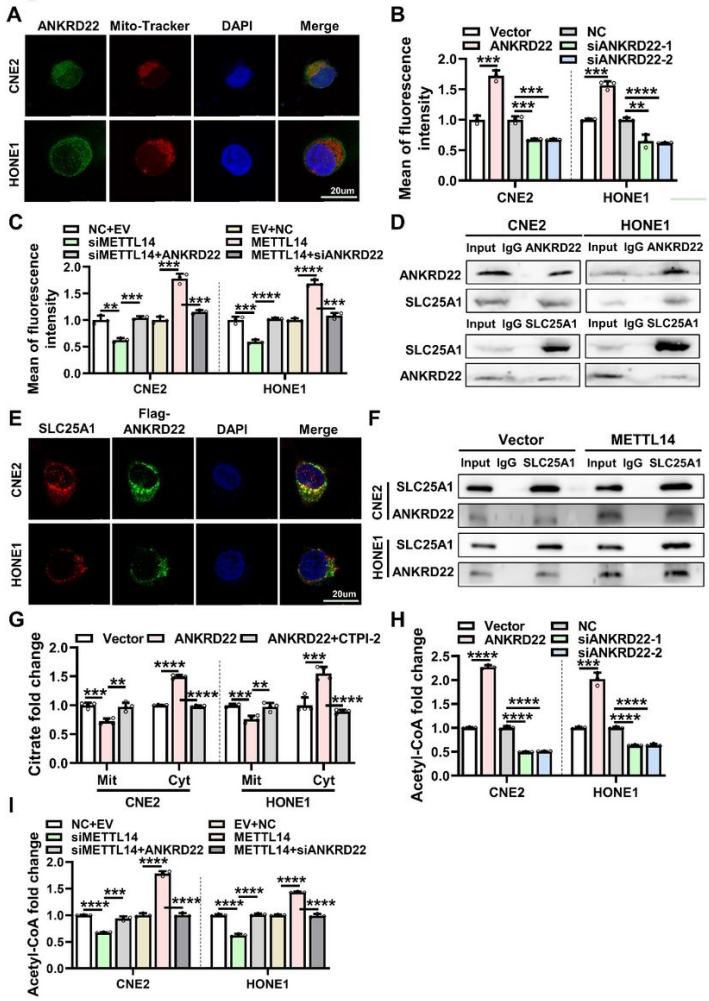

Figure 6

METTL14 prompts lipid metabolism in NPC cells by upregulating ANKRD22 expression

A. IF assays showed co-localization of ANKRD22 (green) and mitochondria (red) in the cytoplasm in CNE2 and HONE1 cells. Cell nuclei were counterstained with DAPI (blue). Scale bar: 20 μm.

B.Flow cytometry assaying lipid content after overexpression or knockdown of ANKRD22 in CNE2 and HONE1 cells. The original data are shown in Supplementary Fig. 7B.

C.Flow cytometry assays assaying lipid content after co-transfection of METTL14 siRNA and ANKRD22 overexpression vector or co-transfection of METTL14 overexpression vector and ANKRD22 siRNA in CNE2 and HONE1 cells. The original data are shown in Supplementary Fig. 7D and Supplementary Fig. 7E.

D. Co-IP assays analyzing the interaction between ANKRD22 and SLC25A1 in CNE2 and HONE1 cells using anti-ANKRD22 antibody (upper panel) or anti-SLC25A1 antibody (lower panel).

E. IF assays showing co-localization of SLC25A1 (red) and Flag-ANKRD22 (green) in the cytoplasm in CNE2 and HONE1 cells. Cell nuclei were counterstained with DAPI (blue). Scale bar: 20 μm.

F.Interaction between ANKRD22 and SLC25A1 after overexpression of METTL14 in CNE2 and HONE1 cells was detected by IP using anti-SLC25A1 antibody.

G. Citrate assay kit was used to detect the effect of overexpression of ANKRD22 and treatment with CTPI-2 on citrate contents in mitochondria and cytoplasm in CNE2 and HONE1 cells. Mit: mitochondrion, Cyt: cytoplasm.

H. Acetyl-CoA assay kit was employed to measure acetyl-CoAcontent after overexpression or knockdown of ANKRD22 in CNE2 and HONE1 cells.

I. Acetyl-CoA assay kit was employed to measure acetyl-CoA contents in CNE2 and HONE1 cells after co-transfecting with METTL14 siRNA and ANKRD22 overexpression vector or co-transfecting with METTL14 overexpression vector and ANKRD22 siRNA.

Data were presented as mean ± SD. $^{**}p < 0.01$, $^{***}p < 0.001$, $^{****}p < 0.0001$.

Fig. 7

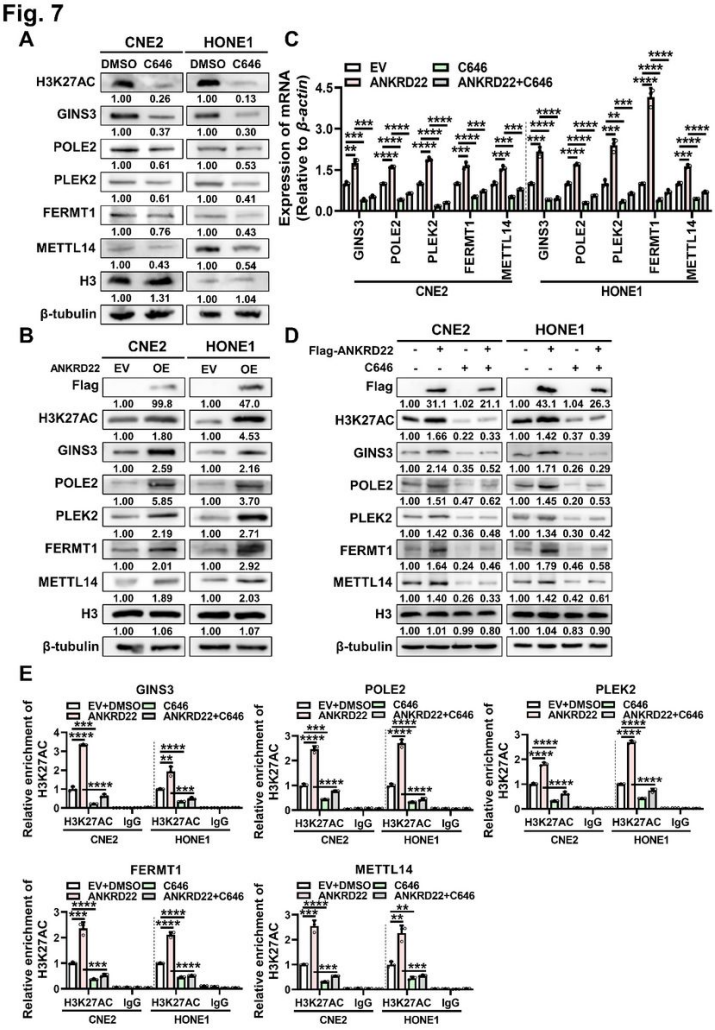

Figure 7

ANKRD22 activates downstream gene transcription through enhancing H3K27AC

A.Protein levels of H3K27AC, GINS3, POLE2, PLEK2, FERMT1, and METTL14 in CNE2 and HONE1 cells after treatment with C646 (20 μM) were detected by western blotting.

B.Protein levels of H3K27AC, GINS3, POLE2, PLEK2, FERMT1, and METTL14 in CNE2 and HONE1 cells after overexpression of ANKRD22 were detected by western blotting.

C, D.GINS3, POLE2, PLEK2, FERMT1, and METTL14 mRNA (**C**) and protein (**D**) levels in CNE2 and HONE1 cells after overexpression of ANKRD22 and treatment with C646 (20 μM) were detected by RT-qPCR and western blotting, respectively.

E.ChIP-qPCR assays evaluating H3K27AC enrichment near the promoters of GINS3, POLE2, PLEK2, FERMT1, and METTL14 in CNE2 and HONE1 cells after overexpression of ANKRD22 and treatment with C646 (20 μM).

Data were presented as mean ± SD. $^{**}p < 0.01$, $^{***}p < 0.001$, $^{****}p < 0.0001$.

Fig. 8

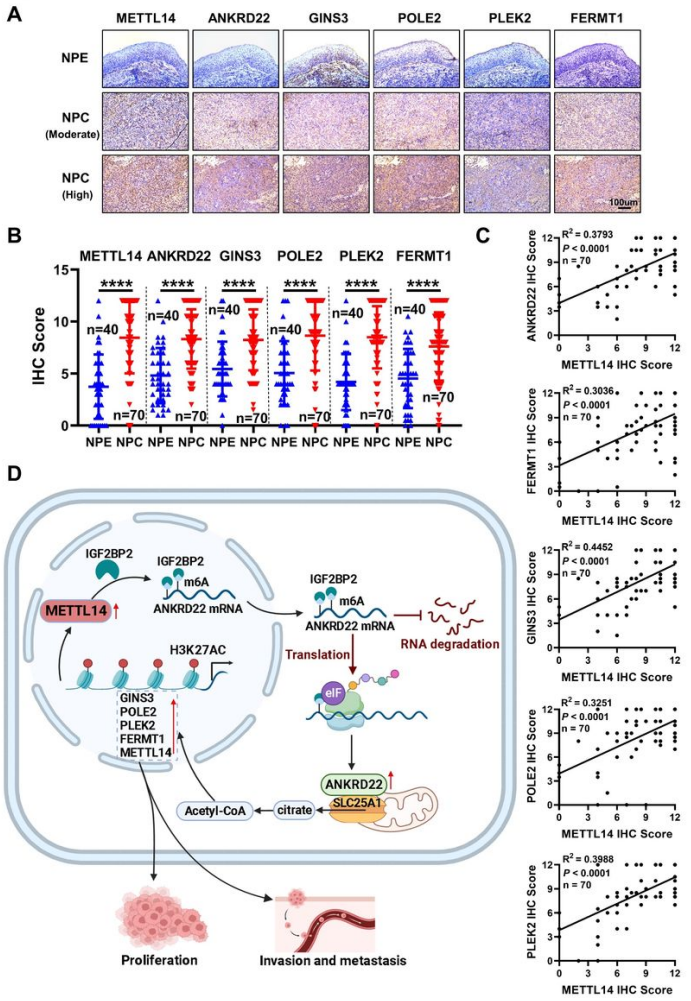

Figure 8

Positive correlations between METTL14 and ANKRD22 along with its downstream genes in NPC clinical samples

A. IHC assays evaluating the expression levels of METTL14, ANKRD22, GINS3, POLE2, PLEK2, and FERMT1 proteins in 70 NPC tissues and 40 adjacent NPE tissues. Scale bar: 200 ×, 100 μm.

B. Statistical analysis of METTL14, ANKRD22, GINS3, POLE2, PLEK2, and FERMT1 expression in 70 NPC tissues and 40 adjacent NPE tissues.

C. Correlation between METTL14 and ANKRD22, GINS3, POLE2, PLEK2, FERMT1 in 70 NPC tissues.

D. Diagram illustrating the mechanism by which METTL14 promotes malignant progression of NPC through upregulation of m^6A modification of ANKRD22.

Data were presented as mean ± SD. ****$p < 0.0001$.

Supplementary Files

This is a list of supplementary files associated with this preprint. Click to download.

- SupplementaryTable1.Clinicopathologicaldatafor28NPCand7NPEtissuesusedforqRTPCR.xlsx
- SupplementaryTable2.Clinicopathologicaldataon80paraffinembeddedNPCtissuesandtheexpressionofMETTL14ANKRD22inthesesamplesmeasuredbyimm
- SupplementaryTable3.Clinicopathologicaldataon70paraffinembeddedNPCtissuesandtheexpressionofMETTL14ANKRD22GINS3POLE2PLEK2andFERMT1
- SupplementaryTable4.ListofsiRNAs.xlsx
- SupplementaryTable5.ListofqRTPCRprimers.xlsx
- SupplementaryTable6.Listofprimaryantibodiesforimmunohistochemistrywesternblottingm6Adotblotimmunofluorescenceimmunoprecipitationand ChIP.xls
- SupplementaryTable7.Listof739geneswithbothdifferentialm6Alevelsanddifferentialm RNAlevels.xlsx
- SupplementaryTable8.ListofgenesinGSE12452withacorrelationcoefficientgreaterthan0.5withANKRD22.xlsx

- SupplementaryFigs.docx